

ERO R1 in CL0939+4713 field

- Evidence for an S0-like galaxy at $z \sim 1.5^1$

Masanori IYE^{2,3}, Kazuhiro SHIMASAKU⁴, Satoshi MIYAZAKI⁵,
 Masatoshi IMANISHI², Nobunari KASHIKAWA^{2,3}, Tadayuki KODAMA⁴,
 Masashi CHIBA^{2,3}, Yoshihiko SAITO², Miwa GOTO⁶,
 Fumihide IWAMURO⁷, Naoto KOBAYASHI⁸, Sadanori OKAMURA⁴,
 Chris SIMPSON⁸, and Hiroshi TERADA⁸

iye@optik.mtk.nao.ac.jp

ABSTRACT

We report that an extremely red galaxy, ERO R1 with $R - K = 7.4$, identified in the field behind the cluster of galaxies A851 (=Cl 0939+4713) at $z = 0.4$ was shown to be a disk galaxy at $z \sim 1.5$ with passively evolving stellar population, placing it the most distant S0-like galaxy ever observed. Its redshift was derived consistently from two independent methods; the photometric redshift method based on its $V, R, F702W, i, J, H$, and K' magnitudes using the HYPERZ code and the cross correlation method using its H -band spectrum and the optical spectra of local E/S0 galaxies. Although its colors are consistent both with an elliptical galaxy and an S0 galaxy at that redshift, its elongated shape indicates the S0-like nature of this galaxy and the measured exponential luminosity profile of this galaxy clearly shows its resemblance to the present day disk galaxies. The possible effect of the gravitational stretching due to the foreground cluster is not strong enough to explain its elongated shape and above all the lensing does not affect the shape of the luminosity profile. We, therefore, defy the interpretation of a lensed elliptical galaxy. The H -band spectrum does not show conspicuous redshifted $H\alpha$ emission and the star forming activity in this galaxy, if any, appears to be very modest. The presence of such a galaxy with apparently dynamically relaxed disk system of stars at that high redshift poses a new constraint on theoretical models to explain the formation and evolution of galaxies.

Subject headings: galaxies: clusters: individual(A851)—galaxies: ellipticals and lenticulars, cD—galaxies: evolution

²Optical and Infrared Astronomy Division, National Astronomical Observatory, Mitaka, Tokyo 181-8588

³Department of Astronomy, School of Science, Graduate University for Advanced Studies, Mitaka, Tokyo 181-8588

⁴Department of Astronomy, School of Science, University of Tokyo, Bunkyo-ku, Tokyo 113-0033

⁵Advanced Technology Center, National Astronomical Observatory, Mitaka, Tokyo 181-8588

⁶Institute for Astronomy, University of Hawaii, North A'Ohoku Place, Hilo, HI 96720, USA

⁷Department of Astronomy, Kyoto University, Kitashirakawa, Kyoto 606-8502

⁸Subaru Telescope, National Astronomical Observatory, 650 North A'Ohoku Place, Hilo, HI 96720, USA

⁸Based on data collected at Subaru Telescope, which

1. Introduction

The cluster of galaxies A851 (= Cl0939+4713) at $z = 0.4$ was observed during the first light period of Subaru Telescope using the optical imager, Suprime-Cam, and the infrared imager, CISCO, both mounted at the Cassegrain focus (Iye et al. 2000). Among the five EROs with $R - K' > 5$ found in the cluster field, the object ERO R1 called our special attention for its outstanding color $R - K' = 7.4$ and the elongated shape,

is operated by the National Astronomical Observatory of Japan.

$b/a = 0.4$, with its major axis aligned with the equipotential surface of the cluster. The object ERO R1, at $\alpha = 09^h42^m58.6^s$ and $\delta = 46^\circ59'12''$, was referred to for the first time in the literature in the footnote of Smail et al. (1999) as object # 333. Figure 1 shows the postage stamp images of ERO R1 in various bands.

Preliminary analysis by comparing its R , J , and K' magnitudes in the color – magnitude diagrams with various evolution models of galaxies with varying amount of dust extinction suggest that this object is likely to be an early type galaxy with passive evolution at $1.0 < z < 1.6$ with modest dust extinction ($E(B - V) < 0.5$). The direction of the elongation of this image suggested a possibility that it is a gravitationally lensed image of a rounder background galaxy. On the other hand, the smooth and symmetrical shape indicates it being an intrinsic S0 galaxy or a disk galaxy rather than a lensed image of background elliptical.

Whether the object ERO R1 is really an early type galaxy with dynamically relaxed disk component of stars or not is an important issue from the point of formation scenario of galactic disks. We attempted to make follow up observations to elucidate the nature of this object and report the results obtained from our studies. We adopt the cosmological model with $H_0 = 70$ km/s/Mpc, $\Omega = 0.3$, and $\Lambda = 0.7$ throughout this paper unless otherwise mentioned.

2. Observations and reduction

2.1. IRCS spectroscopy and imaging

On Feb. 2, 2001, the InfraRed Camera and Spectrograph, IRCS, was used to observe the ERO R1. The H -band images of 2 minute exposure were obtained at 5 slightly offset pointings for three sets, yielding a total of 30 minute exposure. Similarly, 4 sets of 2 minute zJ -band images at 5 pointings were obtained to secure a total of 40 minute exposure time. The zJ -band referred here is characterized by a filter with a band width $0.073 \mu m$ centered at $1.033 \mu m$. The sky condition was clear and the seeing was $0.^{\prime\prime}45 - 0.^{\prime\prime}60$. The standard star FS127 (Hawarden 2001) was observed as a photometric zero-point calibrator.

On the same night, we obtained low-resolution grism spectra with a $0.^{\prime\prime}9$ slit covering the H -band

at a spectral resolution $R \sim 100$. The slit was aligned to the major axis of ERO R1 at PA 139° and the $20''$ portion along the slit was exposed. To minimize the effect of detector non-uniformity, exposures were made alternatively by positioning the target object at two positions separated by $7''$ along the slit by nodding the telescope. A total of 44 exposures of 5 minute each were secured giving the total on-source exposure time of 220 minute. HR1729, HR3928, and HR4761 were observed as spectrophotometric standard stars. The IRCS observation was made with considerable over-sampling of $0.^{\prime\prime}06/\text{pixel}$ due to its design configuration optimized for high spatial resolution imaging and spectroscopy. The signal to noise ratio of the object was, therefore, not sufficiently high for accurate spectrophotometry.

2.2. IRCS data reduction

As for the H - and zJ - band imaging data, standard data analysis procedures were employed, using IRAF ⁹.

First, bad pixels were removed and the values of these pixels were replaced with values interpolated from the surrounding pixels. Second, the frames were dark-subtracted and then scaled to have the same median pixel value, so as to produce a flat frame. The dark-subtracted frames were then divided by a normalized flat frame to produce images at each dithering position. Images were aligned to sub-pixel accuracy using a bright source near to ERO R1, and then combined to produce the final image.

For calibrating the H -band spectra, we chose an F-type standard star HR 4761 (F6–8V) observed with an air mass difference of <0.1 from the target source ERO R1 to correct for the transmission of Earth's atmosphere. We used the task *apall* in IRAF to extract the spectra of ERO R1 and HR 4761. Signals over $2''$ along the slit were integrated. Wavelength calibration was performed using the argon lamp lines and the sky lines. The spectrum of ERO R1 was divided by that of HR 4761, and was multiplied by the spectrum of

⁹IRAF is distributed by the National Optical Astronomy Observatories, which are operated by the Association of Universities for Research in Astronomy, Inc (AURA), under a cooperative agreement with the National Science Foundation.

the blackbody radiation with temperature corresponding to HR 4761 (T = 6200K). After applying the flux calibration based on the H -band photometry, the final spectrum was produced.

2.3. Aperture Photometry

The B, V, R, I Suprime-Cam imaging observation of A851 at the prime focus of the Subaru Telescope was carried out on January 21 and 22, 2001 to study the large scale structure in the distribution of galaxies in this field (Kodama et al. 2001). The photometry of ERO R1 in these frames were carried out to supplement data on the V - and I -bands to give better constraints on photometric redshift analyses. The logs of IRCS and Suprime-Cam observations of ERO R1 are summarized in table 1. The image in B -band was taken under a poor seeing and didn't allow precise photometry of ERO R1. We retrieved the NICMOS/HST H -band archived image obtained by (Smail et al. 1999) to supplement our H -band imaging.

The photometry of ERO R1 with a circular aperture of $4''$ diameter on all the available bands, including those obtained in 1999, was carried out using the identical parameter settings of the SExtractor. The R , J , and K' magnitudes given in the previous paper (Iye et al. 2000) were mag(best) derived by the SExtractor and are slightly, but not much, different from the present results of mag(4 arcsec). As for the calibration of the zero point of the NICMOS H -band data, we used the published magnitude of an unblended galaxy in the image. The photometric results of ERO R1 in Vega magnitude scale are given in table 2.

3. Properties of ERO R1

3.1. Luminosity profile

We analyze the structure of the ERO R1 based on its K' -band image because it has the highest S/N ratio, the best seeing, and the least extinction and is appropriate for studying the stellar light at $z \sim 1.5$. The isophotal image size of ERO R1 at $K' = 22$ mag/arcsec 2 is $3''.7 \times 1''.8$, corresponding to $22 \times 11h^{-1}$ kpc at $z = 1.5$, which is fairly large but not exceedingly. The luminosity profile for equivalent radius is consistent with the exponential law as shown in Figure 2. The effect of seeing was checked separately and was found that the seeing effect is fully negligible for $r > 0.''5$. The

K' -band scale length α^{-1} of the exponential disk, corresponding to that of rest frame $0.85\mu m$ -band, is about $2.1 h^{-1}$ kpc. This is consistent with the $F814W$ scale length distribution of CFRS/LDSS redshift survey sample galaxies at $0.2 < z < 1.0$ studied by (Lilly et al. 1998), where 48 out of 104 galaxies had scale length $\alpha^{-1} > 1.6h^{-1}$ kpc.

By taking the distance modulus, K-correction, and E-correction to the observed K' magnitude into account, we evaluate that the absolute magnitude, which ERO R1 will have at $z = 0$ if it evolves passively, is $M_K = -24.2 + 5logh$. The evolutionary dimming from $z = 1.5$ to $z = 0$ amounts to be about 1 magnitude. The derived absolute luminosity corresponds about $2L_*$ at $z = 0$.

The decomposition of the bulge component from the disk component is a natural interest to study the internal structure of this object. Although the K' -band data under $0''3$ seeing does not allow such a detailed analysis, the slight excess by 0.5 magnitude or less at the center with respect to the seeing convolved exponential profile is likely due to the modest contribution of the bulge component. The luminosity profile of ERO R1 is therefore consistent with those of nearby S0 galaxies having small bulges. Note that gravitational lensing may deform the shape of the image but will not change the exponential profile into a de Vaucouleurs profile.

There is no indication on the presence of overall color gradient or of the dust layer confined to the galactic plane in the image of this galaxy.

Moriondo et al. (2000) made a morphological study of 41 EROs. Most of these objects belong to elliptical like objects. A few galaxies characterized by a compact morphology, however, are best fitted by an exponential distribution. ERO R1 studied in the present paper has an elongated shape that is comparable to the most elongated object, ID 22, among their sample. However, ERO R1 is smoother in its light distribution than any similar objects among their sample.

3.2. Spectral energy distribution

Figure 3 shows the $V, R, F702W, i, J, H$, and K' band photometry of ERO R1 overlaid on the SED of a 1 Gyr elliptical/S0 galaxy at $z = 1.46$ with an extinction $A_V = 1.4$, that was derived by the HYPERZ code (Rodighiero et al. 2000; Bolzenella

et al. 2000) as the best fit model. The estimated error of the derived redshift is ± 0.03 and ± 0.11 at 90% and 99% confidence level, respectively. Note the remarkable fit between the measured magnitudes and the best fit SED model. The second best solution was a 1.4Gyr elliptical/S0 galaxy at $z = 1.59$ with an extinction $A_V = 0.8$ and HYPERZ code concluded as the weighted mean solution a redshift at $z = 1.49$. Anyway, the observed SED with extinction $A_V \leq 1.4$ is not consistent with the SEDs of dusty starbursts, one of the two major populations of EROs, at any redshift. The observed flux in the V -band corresponds to that for the rest UV flux and we see no UV up-turn in ERO R1. The possible contribution of UV up-turn observed in the local elliptical galaxies are mainly from evolved asymptotic giant stars and would not be a significant contribution for a galaxy at $z = 1.5$.

The location of ERO R1 plotted in the $(R - K, J - K)$ two-color diagram to discriminate ellipticals and dusty starbursts (Pozzetti and Mannucci 2000; Mannucci et al. 2001) also indicates that ERO R1 is not a dusty starburst but a passively evolving galaxy. This is consistent with the fact that we did not find redshifted emission line in the H -band spectrum as will be reported in the next section.

3.3. H -band spectrum

H -band spectra were secured to search for a redshifted $H\alpha$ emission. The signal to noise ratio was rather poor due to the over-sampling of the IRCS, which was the only available instrument at the time of observation. After making all the effort to calibrate pixel non-uniformity and other effects, we obtained the resulting SED over the H -band as show in figure 4, where a spectrum of a local elliptical galaxy redshifted to $z = 1.5$ is overlaid for showing the TiO absorption features seen in the $600 - 800$ nm region of the rest frame spectrum. No conspicuous emission line was confirmed in this SED, except for a modest enhancement at 1.5σ level at $1.7\mu m$, which might naively be ascribed to the $H\alpha$ emission at $z = 1.5$. Since the S/N and the spectral resolution of our H -band spectrum were both limited, we can place only a very loose upper limit for the $H\alpha$ flux at about $1 \times 10^{-16} ergs^{-1} cm^{-2}$. However, considering the modest amount of extinction derived in the previous

photometric analysis, we conclude that the starburst activity, if any at all, in this galaxy is taking place only at a very modest level.

A cross correlation analysis was applied between the observed H -band spectrum of ERO R1 and typical spectra of galaxies of type from ellipticals to late type spirals with various ages. Typical example of the resulting correlation function is given in figure 5. The best fit was found for a 3 Gyr single burst passive evolution model of galaxies at the first peak redshift at $z = 1.50 \pm 0.02$ and the second peak at $z = 1.72 \pm 0.02$. Note that 1Gyr elliptical/S0 model at $z = 1.5$ derived as the best fit solution of the HYPERZ code does not give a striking peak in the correlation function. This might reflect the fact that the TiO absorption features do not develope well at 1Gyr and the bumps in the observed H -band SED suggest an age of ERO R1 equal or larger than about 2 Gyr.

4. Discussion

4.1. Clustering around $z = 1.5$?

Daddi et al. (2001) found a strong clustering trend of EROs from their 400 survey samples and argued that EROs constitute large scale clustering population of elliptical galaxies at $z > 1$.

Kodama et al. (2001) made a Suprime-Cam imaging of the CL0939+4713 to study the large scale structure in the distribution of galaxies. They made photometric redshift analysis for most of the identified objects and spectroscopic redshift measurement for some of the objects. The redshift distribution derived in their study shows a slight excess in number of galaxies at $z = 1.5$ and it might suggest the presence of a cluster of galaxies at $z = 1.5$. However, the number enhancement is very modest and the presence of a rich cluster is not yet established. Since the error in photometric redshift evaluation based only on optical images becomes larger for objects at $z > 1$, the possible presence of a cluster behind the A851 should be checked by further studies. A new attempt to make hyperz code analysis using the present R, J, H, K band images supplemented with B and V band images is highly desired to find out if there is any clustering around the ERO R1.

4.2. Evaluation of the lensing effect

Another possibility for understanding the elongated shape of ERO R1 is the image stretching of a background elliptical galaxy by the gravitational lensing of the cluster. Seitz et al. (1996) performed a weak-lensing analysis and found that the cluster mass distribution closely traces the distribution of bright member galaxies in this cluster. Schindler et al. (1998)'s high resolution X-ray observations confirmed the concentration of hot plasma consistent with the weak lensing mass distribution and the distribution of galaxies and indicated that the cluster is still actively evolving towards a virialized state.

The direction of elongation of the ERO R1 image is almost perpendicular to the direction toward the surface mass density peak of the cluster as derived from the weak lensing analysis (Iye et al. 2000). The direction of elongation is therefore consistent with that expected for usual lensing geometry and one can notice the presence of a number of arc-like structures in the HST image of this region.

As ERO R1 resides near the cluster center, 21 arcsec from the optical center of the cluster at ($\alpha = 09^h42^m56.9^s$, $\delta = +46^\circ59'23.1''$: J2000), or 20.4 arcsec from the M1 of the X-ray peak at ($\alpha = 09^h42^m58.2^s$, $\delta = +46^\circ58'52''$: J2000), it is conceivable that the image of ERO R1 can be a gravitationally distorted background galaxy.

In order to have a strong lensing effect incurred on a galaxy at distance r Mpc from the cluster center, a lensing mass of $M(< r) > \pi\sigma_{cr}r^2$ is required, where the critical surface mass density, σ_{cr} , depends on the distances to the lensed sources and to the lensing object and on the cosmological model. Since the redshift to the source ERO R1, $z = 1.5$, and to the lens, $z = 0.4$, are known, one can calculate the lensing mass to be $M(< r) = 1.4 \times 10^{16}r^2M_\odot$, which amounts to be $3 \times 10^{13}M_\odot$ at the distance of ERO R1, $r = 0.044$ Mpc, assuming the center of the cluster to be the location where the reconstructed surface mass density peaks as shown in Figure 13 of (Iye et al. 2000).

Figure 6 shows the integrated radial mass profile of the cluster as derived from the weak lensing analysis using the method described in (Kaiser et al. 1995). The integrated mass $M(< r)$ of the

cluster in the unit of solar mass inside the circle with radius r from the peak position of the reconstructed surface mass shown in Fig 13 of (Iye et al. 2000) is plotted for assumed mean redshift of $z_s = 1.0$ and 3.0, respectively, of the faint background galaxies. Although exact evaluation of the mean redshift of faint galaxies used in this analysis is not available, the curve for $z_s = 1.0$ is more likely to be the case.

The integrated mass of the cluster inside the projected distance to ERO R1 is then at most $1 \pm 0.4 \times 10^{13}M_\odot$, which is about 1/3 of the mass required for strong lensing. The error estimate for the mass depends also to the assumed position of the cluster center. If the cluster center is at the location M1, the primary peak position of the ROSAT X-ray map (Schindler et al. 1998), the distance to ERO R1 becomes about 1.5 times larger and hence the mass required for strong lensing becomes even larger. Separate estimates of the mass were made by displacing the center of the lensing mass to locations in four directions and it was found the error associated in the assumed position of the center is not significant and does not increase the mass by more than 30 %. We, therefore, conclude that the cluster lensing mass is not sufficient to exert a strong lensing effect on ERO R1.

Finally, we show the result of our attempt to reconstruct the unlensed image of ERO R1 at $z = 1.5$ using the singular isothermal sphere mass model of lensing cluster with its total mass taken from (Schindler et al. 1998). Unlensed image of ERO R1 is shown for five cases. Figure 7 (Case 0) gives the unlensed image when the center of the lensing cluster is placed at the peak M1 of the extended X-ray emission. Since the X-ray map is smoothed by a Gaussian beam of 10 arcsec, we show further the unlensed images for four cases in Figure 8, where the lensing cluster is displaced by $10''$ from the extended X-ray peak position M1 in four directions; Case N(to the north), Case W(west), Case E(east), and Case S(south), respectively. The unlensed image for Case N has a region where the observed data is not available and the lowest surface brightness was assigned. We performed surface photometry with these unlensed images and confirmed that unlensing does not change the light profile and the light profile of unlensed image of ERO R1 is well represented

by the exponential profile, as is expected. Therefore, the exponential profile of ERO R1 suggests strongly the presence of a disk component in this galaxy at $z = 1.5$ and that the elongated image of ERO R1 is not a gravitationally stretched image of an elliptical galaxy.

4.3. S0 galaxies at low and intermediate redshift

Poggianti et al. (2001) studied the ages of stellar populations in 52 elliptical and S0 galaxies in the Coma cluster and found that more than 40% of the S0's have undergone star formation in their central regions during the last ~ 5 Gyr, where as such activity is absent in the ellipticals.

MORPHS collaboration (Smail et al. 1997; Dressler 1997), studying the morphology of galaxies in clusters back to the epoch $z \sim 0.5$ using the high resolution images obtained with the *Hubble Space Telescope*, showed that there is a deficit of S0 galaxies in intermediate redshift clusters with respect to nearby clusters. Rodighiero et al. (2001) confirmed from their morphological analysis of galaxies in the HDFN and HDFS that massive E/S0 tend to disappear from flux-limited samples at $z > 1.4$ and that the era $1 < z < 2$ corresponds to a very active phase for the assembly of massive E/S0 galaxies in the field.

On the other hand, the luminous early-type populations of rich clusters are known to be remarkably homogeneous and the bulk of their stellar populations appear to be old (Bower et al. 1992; Ellis et al. 1997). Jones et al. (2000) found from their spectroscopic data that there is no statistically significant difference between the luminosity-weighted age of the E and S0 galaxies in clusters at $0.37 < z < 0.56$. These findings support the conventional formation model of old, coeval E and S0 galaxies.

Part of the cause of the apparent conflict between the above two results was ascribed to the morphological classification error of E and S0 galaxies at $z > 0.5$ (Andreon 1998).

4.4. Examples of disk galaxies at high redshift

The observed colors and the K' magnitude of the ERO R1 are very similar to the extremely red object CL 0939+4713B at $z = 1.58$ found by Soifer

et al. (1999) in the region just southwest of the field covered by the present observation. It is also similar in colors to the extremely red object HR 10 found by Hu & Ridgeway (1994) in the field of PC1643+4631A, which was proposed to be a red-denied galaxy with star formation at $z=1.44$ based on its $H\alpha$ emission identified by Graham & Dey (1996). The noticeably elongated shape of ERO R1 is unique as compared with the modest elongation observed in Cl 0939+4713B or in HR10.

Benitez et al. (1999) found some IR-bright ($H < 25$), high-redshift ($z > 1$) galaxies of later spectral type in the Hubble Deep Field South. Their object SP2 has an exponential profile whereas the SED with UV up-turn implies a spiral galaxy at $z = 1.2$ with minimum age of ~ 1 Gyr.

van Dokkum and Stanford (2001) discovered a rapidly rotating disk galaxy at $z = 1.34$, that shows a redshifted [OII] emission, irregular morphology with patchy regions of star formation, and the luminosity $3L_*$. They classified this object as an Sb/Sc galaxy.

van Dokkum et al. (2001) studied the galaxy population in the IR selected cluster RX J0848+4453 at $z = 1.27$, using deep HST NICMOS and WFPC2 images of the cluster core and classified all the 22 galaxies to $K_s = 20.6$. They found evidence of undergoing merging events in that cluster and suggested that luminous early-type galaxies exist in clusters at $z \sim 1.3$. None of the disk galaxies they found, however, look alike the ERO R1 in A851.

Lilly et al. (1998) made structural analysis of 341 galaxies in the range $0 < z < 1.3$ selected from the CFRS and LDSS redshift surveys using the HST images.

Smith,G. et al (2002) studied the Hubble image of a gravitationally lensed ERO J003707 at $z = 1.6$ in the field of the cluster A68 at $z = 0.255$ and concluded that this object is an L^* early-type disk-galaxy from their reconstructed image and photometric analysis and remarked that the unique association of passive EROs with elliptical galaxies appears to be too simplistic. The present paper presents the data of ERO R1 with significantly higher S/N ratio supporting their view.

4.5. Implications for the early formation of an S0 galaxy

Dressler (1980) found the density morphology relation and the formation of S0 galaxies in nearby clusters are often related to the effect of ram pressure stripping. If there is a massive cluster of galaxies around ERO R1 at $z = 1.5$, the formation of ERO R1 may be ascribed to the ram pressure stripping process that took place in such an early epoch of the universe. In this case, one might be able to detect the redshifted X-ray emission from this background cluster of galaxies.

On the other hand, if there is no such a concentration of galaxies around ERO R1, the formation of ERO R1 should have taken place without recourse to ram pressure stripping and this gives a new challenge to theoretical models to explain the formation of galaxies.

Susa and Umemura (2000a,b) made simulations using their radiative SPH code to show that disk galaxies can be formed if the formation of galaxy took place at $z_F < 2$ under a strong UV radiation field, since the UV background works to prolong the star formation and the gas can fall onto a disk through a dissipative process. They showed that a settled disk galaxy is formed by $z = 1$ under a strong UV background for a model with $z_F = 2$. It is extremely important to make detailed studies of individual galaxies at $z > 1$, to have a consistent scenario of the formation and evolution of galaxies.

5. Summary

The ERO R1 found in the spiral rich cluster A851 (=Cl 0939+4713) at $z = 0.4$ was identified with a passively evolving galaxy at redshift $z = 1.48 \pm 0.02$ by means of photometric redshift analysis based on V, R, i, z, zJ, J, H , and K' bands and a cross correlation analysis of its H -band spectrum. The image stretching effect due to the gravitational lensing of the foreground cluster, though playing a part to some extent, cannot be the main cause of its elongated shape. The K' -band luminosity profile along the major axis is well represented by the exponential disk, indicating that the distribution of the stellar population of this galaxy has already in a dynamically stable configuration. The lack of significant redshifted $H\alpha$ emission and its broad band colors suggest that the star forming activity in this galaxy is very modest. These

findings point that ERO R1 is an S0-like galaxy with well developed and dynamically relaxed stellar disk component at an era of $z = 1.5$. This finding of an S0-like galaxy at $z = 1.5$ poses a new constraint on disk formation scenarios of galaxies at high redshift.

We are grateful to Subaru Telescope staff for supporting the observations reported in the present paper.

REFERENCES

Andreon,S., 1998, ApJ, 501, 533
Benitez,N., Broadhurst,T., Bouwens,R., Silk,J., & Rosati,P., 1999, ApJ, 515, L65
Bolzenella,M., Miralles,J.-M., & Pello,R., 2000, A&A, 363, 476.
Bower,R., Lucey,J., Ellis,R., 1992, MNRAS, 254, 601.
Daddi,E., Cimatti,A., Pozzetti,C., Hoekstra,H., Roettgering,M.J.A., Renzini,A., Zamorani,G., and Mannuri,F. 2000, A&A, 361, 535.
Dressler, A., 1980, ApJ., 236, 351.
Dressler, A., Oemler,A., Couch,W., Smail,I., Ellis,R., Barger,A., Butcher,H., Poggianti,B., & Sharples,R., 1997, ApJ., 490, 577.
Ellis,R., Smail,I., Dressler,A., Couch, Oemler,A., Butcher,H., & Sharples,R., 1997, ApJ, 483, 582.
Graham J.R. and Dey,A. 1999, ApJ. 471, 720.
Hawarden,T., Leggett,S.K., Letawsky,M.B., Ballantyne,D.R., and Casali,M.M., 2001, MNRAS, 325, 563.
Hu E M and Ridgeway S E 1994, AJ. 107, 1303.
Iye,M., Iwamuro,F., Maihara,T., Miyazaki,S., Okamura,S., Shimasaku,K., Simpson, K. et al., 2000, PASJ, 52, 9-23 and PL6-10.
Jones,L., Smail,I., & Couch,W.,J., 2000, ApJ, 528, 118.
Kaiser,N., Squires,G., and Broadhurst,T., 1995, ApJ, 449, 460.

Kodama,T., Smail,I., Nakata,F., Okamura,S., and Bower,R.G., 2001, ApJ, 562, L9.

Lilly,S., Schade,D., Ellis,R., Le Fevre,O., Brinchmann,J., Tresse,L., Abraham,R., Hammer,F., Crampton,D., Colless,M., Glazebrook,K., Mallen-Orneals,G., Broadhurst,T., 1998, ApJ, 500, 75.

Mannucci,F., Pozzetti,L., Thompson,D., Oliva,E., Baffa,C., Comoretto,G., Gennari,S., and Lisi,F., 2001, MNRAS, 327, L57.

Moriondo,G., Cimatti,A., and Daddi,E., 2000, A&A, 364,26.

Poggianti,B.M., Bridges,T.J., Carter,D., Mobasher,B., Doi,M., Iye,M., Kashikawa,N. et al., 2001, ApJ, 563, 118.

Pozzetti, L. and Mannucci, F., 2000, MNRAS, 317, L17.

Rodighiero,G., Franceschini,A., & Fasano,G., 2001, MNRAS, 324, 491.

Rodighiero,G., Granato,G.L., Franceschini,A., Fasano,G., and Silva,L., 2000, A&A, 364, 517.

Schindler S., Belloni P., Ikebe Y., Hattori M., Wambsganss J., and Tanaka Y. 1998, A&A 338, 843.

Seitz,C., Kneib,J.P., Schneider,P. and Seitz,S. 1996, A&A, 314, 707.

Smail,I., Dressler,A., Couch,W.J., Ellis,R., Oemler,A., Butcher,H., and Sharples,R.M., 1997, ApJS, 110, 213.

Smail I, Morrison G, Gray M E, Owen F N, Ivison R J, Kneib J-P, Ellis R S 1999, ApJ, 525, 609.

Smith,G.P., Smail,I., Kneib,J.P., Davis,C.J., Takamiya,M., Ebeling,H., and Czoske,O., 2002, astroph0203402.

Soifer,B.T., Matthews,K., Neugebauer,G., Arimus,L., Cohen,J.G., and Persson, S.E. 1999, AJ, 118, 206.

Susa,H. and Umemura,M., 2000, MNRAS, 316, L17.

Susa,H. and Umemura,M., 2000, ApL, 537, 578.

van Dokkum,P.G., Stanford,S.A., Holden,B.P., Eisenhardt,P.R., Dickinson,M., and Elston,R., 2001, ApJ, 552, L101.

van Dokkum,P.G. and Franx,M., 2001, ApJ, 553, 90.

van Dokkum,P.G. and Stanford,S.A., 2001, ApJ, 562, L35.

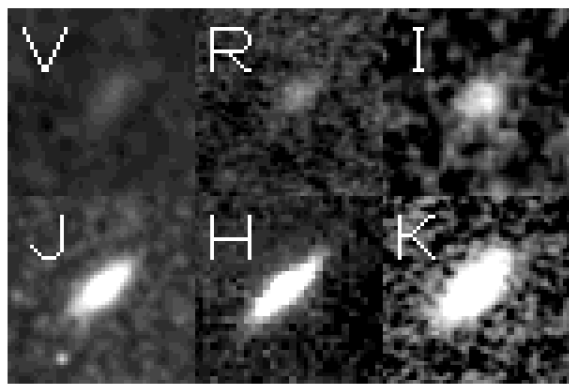


Fig. 1.— K' , H , J , zJ , I , R , and V images of ERO R1

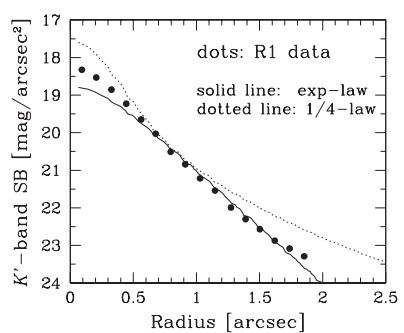


Fig. 2.— K' band luminosity profile along the major axis of ERO R1.

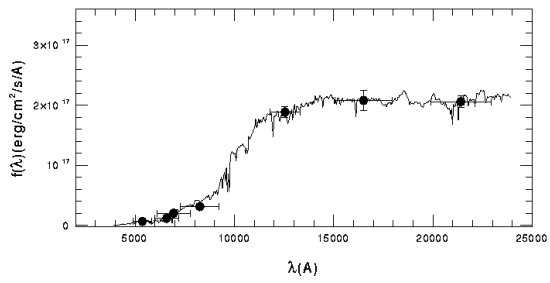


Fig. 3.— Broad band photometry of ERO R1 (filled circles) compared with the best fit evolutionary synthesis model of a 1 Gyr elliptical/S0 galaxy at $z = 1.46$ with the extinction $A_v = 1.4$.

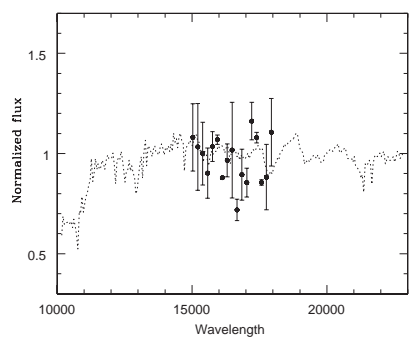


Fig. 4.— H -band SED of ERO R1 (filled circles with error bars) overlaid on a 3 Gyr single burst passive evolution model of galaxy at redshift 1.5 (broken line).

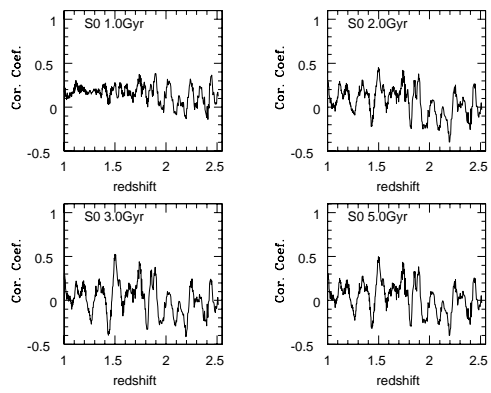


Fig. 5.— Cross Correlation of the H -band SED with single burst passive evolution models of galaxies at various ages.

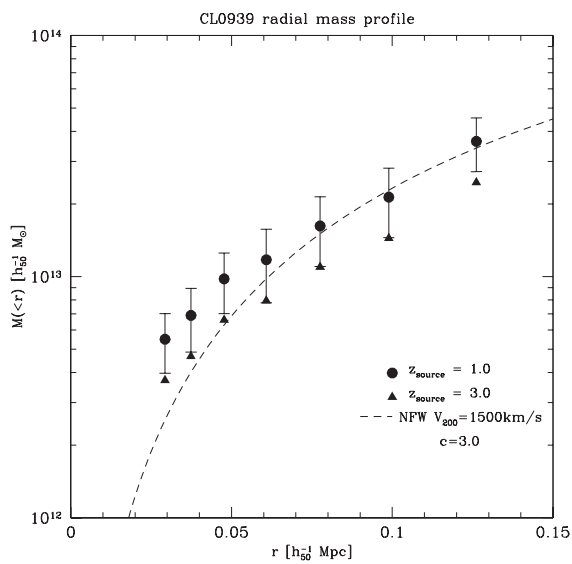


Fig. 6.— Surface mass density distribution of the central region of A851 reconstructed from the weak lensing analysis of Subaru *R*-band data. Contours with solid lines show density enhancement while contours with broken lines show density depression.

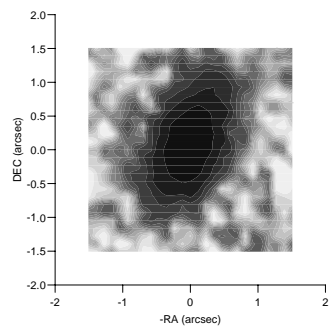


Fig. 7.— Unlensed image of ERO R1 based on an isothermal model for the lensing cluster with its center placed at the X-ray intensity peak M1 (Case 0)

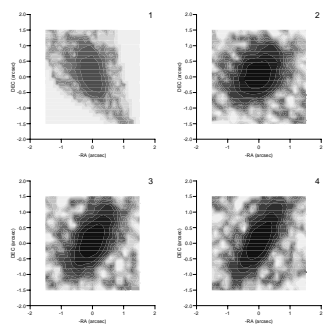


Fig. 8.— Unlensed image of ERO R1 for four other cases with the center of the cluster displaced by $10''$ in N, E, S, and W directions.

Table 1. Observational logs of IRCS and Suprime-Cam.

Date	Instrument(Focus)	Band	Exposure	Seeing	5σ
Jan.21, 2001	Suprime-Cam(Prime)	<i>B</i>	900 s \times 4	1. ^{''} 1	27.0
Jan.22, 2001	Suprime-Cam(Prime)	<i>V</i>	540 s \times 4	0. ^{''} 7	26.3
Jan.12, 1999	Suprime-Cam(Cass)	<i>R</i>	900 s \times 4	0. ^{''} 45	-
Jan.21, 2001	Suprime-Cam(Prime)	<i>R</i>	990 s \times 4	1. ^{''} 1	26.2
Jan 22, 2001	Suprime-Cam(Prime)	<i>I</i>	315 s \times 4	0. ^{''} 7	24.6
Jan.13, 1999	CISCO(Cass)	<i>J</i>	60 s \times 48	0. ^{''} 3	-
Feb.2, 2001	IRCS(Cass)	<i>H</i>	120 s \times 15	0. ^{''} 55	-
Feb.2, 2001	IRCS(Cass)	<i>zJ</i>	120 s \times 20	0. ^{''} 55	-
Jan.11, 1999	CISCO(Cass)	<i>K'</i>	20 s \times 144	0. ^{''} 3	-

Table 2. Photometry of ERO R1.

Band	Magnitude	Error
<i>B</i> Suprime-Cam	-	-
<i>V</i> Suprime-Cam	26.48	0.22
<i>F702W</i> WFPC2	24.86	0.06
<i>R</i> Suprime-Cam	25.59	0.05
<i>I</i> Suprime-Cam	23.78	0.12
<i>zJ</i> IRCS	21.1	0.24
<i>J</i> CISCO	20.47	0.01
<i>H</i> NICMOS	19.24	0.01
<i>H</i> IRCS	19.40	0.09
<i>K'</i> CISCO	18.32	0.01